JOURNAL OF Materials CHEMISTRY

Phase separation behavior and magnetic properties of $Li(Fe_xAl_{1-x})_5O_8$ solid solutions

Shuichi Arakawa,* Seiji Toinaga and Shinsuke Hayashi

Toyota Technological Institute, 2-12-1 Hisakata, Tempaku-ku, Nagoya 468-8511, Japan

Phase separation behaviour and magnetic properties of $Li(Fe_xAl_{1-x})_5O_8$ solid solutions have been investigated. A single-phase $Li(Fe_{0.5}Al_{0.5})_5O_8$ solid solution, which was quenched from 1250 °C, separated into Fe-rich and Al-rich solid solution phases with a continuous compositional variation when it was annealed at 1000 and 950 °C inside the chemical spinodal estimated using the theory of Cook and Hilliard. On the other hand, a $Li(Fe_{0.68}Al_{0.32})_5O_8$ solid solution showed binodal-type phase separation after an incubation period of 200 h at 1000 °C inside the miscibility gap but outside the spinodal. The coercive force of the $Li(Fe_{0.5}Al_{0.5})_5O_8$ solid solution spinodally decomposed at 1000 °C increased to 7.2 kA m^{-1}, which was about 9 times as large as that before annealing. Annealing of the $Li(Fe_{0.5}Al_{0.5})_5O_8$ solid solution at 950 °C raised the coercive force to 8.6 kA m^{-1}. The increase in the coercive force is possibly due to the modulated structure which is characteristic of spinodally decomposed ceramics. The coercive force of the $Li(Fe_{0.68}Al_{0.32})_5O_8$ solid solution remained constant even after it was annealed at 1000 °C for 200 h to decompose it binodally.

Various properties of ceramics, such as electrical conductivity and magnetic coercive force, depend strongly on the microstructures as well as the inherent properties of the phases present. In order to modify the properties, much research on the microstructure control of ceramics has been carried out in recent years. Phase separation, such as binodal decomposition (nucleation-growth process) and spinodal decomposition, has been known to evolve a fine texture. There are major differences in thermodynamics, kinetics and morphology between the materials resulting from binodal decomposition and spinodal decomposition.

The nucleation-growth process occurs in the region of the free energy-composition field where the curvature is positive, *i.e.*, $\partial^2F/\partial C^2>0$. When a nucleus increases in size, a positive change in free energy is needed, and this free energy barrier must be surmounted before growth can occur. On the other hand, spinodal decomposition has no thermodynamic barrier, and the single-phase solid solution is unstable to the smallest fluctuation in concentration within the spinodal region of $\partial^2F/\partial C^2>0$. The compositions of the separated phases vary continuously with time until equilibrium compositions are reached. The nucleation-growth process results in distinctly separated particles of a new phase. In contrast, a distinctive feature of spinodal decomposition is the formation of a modulated microstructure with the nanometer-sized wavelength. From this point of view, spinodal decomposition has been studied as an attractive technique for microstructure control in TiO_2–SnO_2,[1–4] $CoFe_2O_4$–Co_3O_4,[5–7] AlN–SiC[8–10] and Al_2O_3–Cr_2O_3–Fe_2O_3[11] systems.

The phase diagram of the $LiAl_5O_8$–$LiFe_5O_8$ system reported by Strickler and Roy[12] shows the presence of a miscibility gap with a critical temperature of 1180 °C. So far as we know, however, no work except that on the kinetics of phase transformation by Kim *et al.*[13] has been performed on this system. $LiFe_5O_8$ is a ferrimagnetic material with an inverse-spinel type crystal structure, and a number of studies on its electrical and magnetic properties have been reported.[14–18] This paper focuses on the phase separation phenomenon of $Li(Fe_xAl_{1-x})_5O_8$ spinel solid solutions and discusses its phase separation behaviour and its magnetic properties.

Experimental

Sample preparation

The $Li(Fe_xAl_{1-x})_5O_8$ solid solutions were prepared by a solid-state sintering method. The starting materials, Fe_2O_3, Al_2O_3 and Li_2CO_3, were uniformly mixed in an appropriate ratio. The mixture was uniaxially pressed at 9.8 MPa into a disc 13 mm in diameter and about 2 mm in thickness, and then isostatically pressed at 290 MPa. After the disc was embedded in powder of the same composition in a Pt crucible, it was sintered at 1250 °C for 10 h in air. The sintered sample was quenched to room temperature. Single phase solid solutions were obtained for all the compositions in this system. We selected the compositions of $x=0.50$ and 0.68 to clarify the difference between spinodal and binodal decomposition behaviour. They were annealed at 950 or 1000 °C for various periods up to 400 h in air and then quenched to room temperature.

Characterization

The phase separation behavior was examined by X-ray diffraction (XRD) analysis with Co-Kα radiation. Lattice parameters of as-sintered and annealed samples were determined from the (220) reflection, using Si as an internal standard. Magnetic properties were measured at room temperature using a vibrating sample magnetometer (VSM) with a maximum applied magnetic field of 40 kA m^{-1}. The coercive force (H_c), saturation magnetization (σ_s) and remnant magnetization (σ_r) were determined from hysteresis loop measurements. The microstructure was observed by scanning electron microscopy (SEM).

Results and Discussion

Phase separation behavior of $Li(Fe_xAl_{1-x})_5O_8$ solid solution

Fig. 1 shows the phase diagram of the $LiAl_5O_8$–$LiFe_5O_8$ system proposed by Strickler and Roy.[12] The broken line is a chemical spinodal that we calculated from eqn. (1).[19]

$$C_s-C_c\approx(C_e-C_c)(1-0.422T/T_c) \quad (1)$$

C_e and C_s are the equilibrium composition and the spinodal composition, respectively. We took a value of 50 mol% as the critical composition C_c and 1453 K as the critical temperature T_c. Annealing conditions (● and ▲) are also shown in Fig. 1.

Fig. 2 shows that the lattice parameter of the single-phase solid solutions increased with increasing x and obeyed Vegard's law. The lattice parameter values were in good agreement with those reported by Kim *et al.*[13]

Fig. 3(a) shows the change in the (220) peak of the $Li(Fe_{0.5}Al_{0.5})_5O_8$ solid solution with annealing time at 1000 °C.

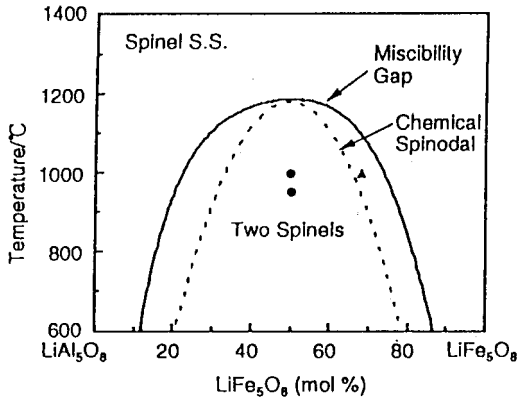

Fig. 1 Phase diagram in the $LiAl_5O_8$–$LiFe_5O_8$ system after Strickler and Roy.[12] Symbols denote the annealing conditions: ● spinodal decomposition, ▲ binodal decomposition.

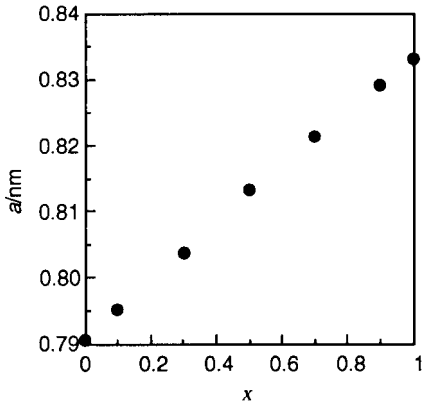

Fig. 2 Lattice parameter of single-phase $Li(Fe_xAl_{1-x})_5O_8$ solid solutions as a function of composition

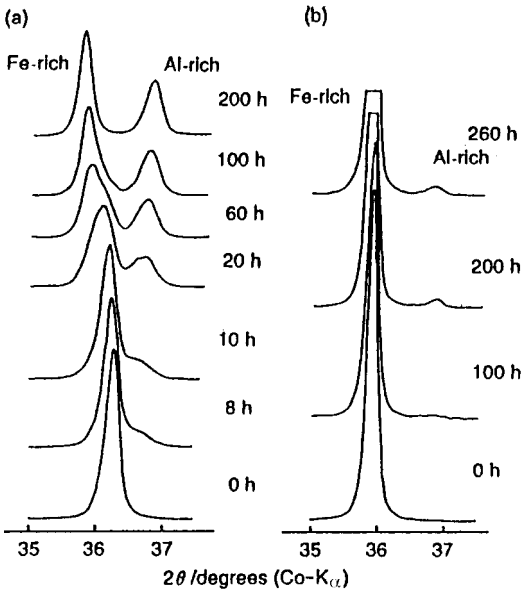

Fig. 3 Change in the (220) peak of $Li(Fe_xAl_{1-x})_5O_8$ solid solutions with annealing time at 1000 °C. (a) $x=0.50$, (b) $x=0.68$.

Upon annealing for 8 h, the (220) peak became broadened slightly and small side peaks appear at the higher angle ($2\theta \approx 36.7°$) and lower angle ($2\theta \approx 36.0°$) sides of the main peak. The side peak positions were difficult to determine precisely in samples annealed for less than 10 h because they overlapped with the main peak. With increasing annealing time, the main peak diminished significantly in intensity, and the intensity of the side peaks continued to increase. The side peaks at the

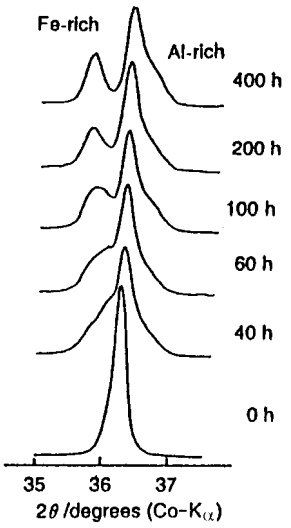

Fig. 4 Change in the (220) peak of the $Li(Fe_{0.5}Al_{0.5})_5O_8$ solid solution with annealing time at 950 °C

higher and lower angles correspond to Al-rich and Fe-rich phases, respectively. The side peak positions moved away from the main peak as the annealing time increased. The splitting of the main peak into two side peaks was completed after annealing for 200 h; the compositions of the coexisting solid solutions in the sample were confirmed from Fig. 2 to reach their equilibrium values at 1000 °C. Fig. 4 indicates that the splitting of the (220) peak to Fe-rich and Al-rich phases also occurs at 950 °C, though the main peak remains after an annealing time of 400 h. This peak is the result of diffraction from the residual undecomposed matrix. Similarly to the result at 1000 °C, the broadening of the main peak was observed in the early stage of annealing. The significant increase in the side peak intensity at 950 °C began at 60 h, while that at 1000 °C began at 20 h; this indicates that the phase separation rate is faster at 1000 °C than at 950 °C.

The change in the (220) peak of the $Li(Fe_{0.68}Al_{0.32})_5O_8$ solid solution with annealing time at 1000 °C is shown in Fig. 3(b). In contrast to $Li(Fe_{0.5}Al_{0.5})_5O_8$, the main peak position for $Li(Fe_{0.68}Al_{0.32})_5O_8$ did not shift until at least 100 h. Two discrete Al-rich and Fe-rich phases appeared after an incubation period of 200 h. Figs. 5 and 6 show the lattice parameters of the main, Fe-rich and Al-rich phases as a function of annealing time at 1000 and 950 °C, respectively. The compositions of the Fe-rich and Al-rich phases for $Li(Fe_{0.5}Al_{0.5})_5O_8$ varied continuously with annealing time. This continuous variation in composition is a feature of the spinodal decomposition, and it is considered that the phase separation observed

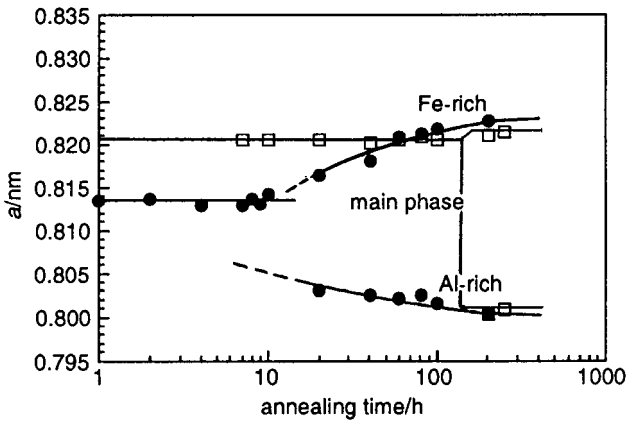

Fig. 5 Variation in lattice parameters for $Li(Fe_xAl_{1-x})_5O_8$ solid solutions as a function of annealing time at 1000 °C. ● $x=0.5$, □ $x=0.68$.

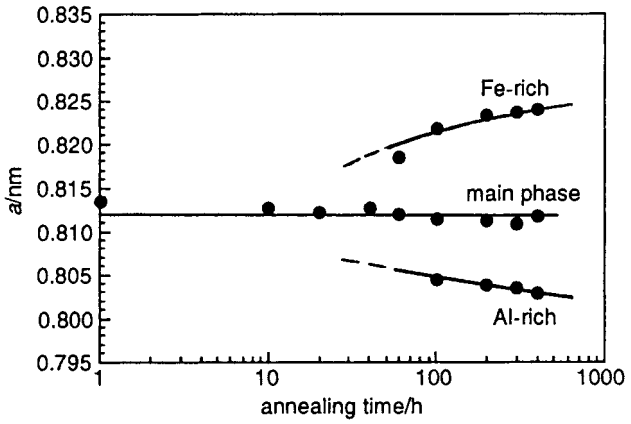

Fig. 6 Variation in lattice parameters for the $Li(Fe_{0.5}Al_{0.5})_5O_8$ solid solution as a function of annealing time at 950 °C

in the $Li(Fe_{0.5}Al_{0.5})_5O_8$ solid solution is in spinodal mode. On the other hand, the formation of the Al-rich phase in the $Li(Fe_{0.68}Al_{0.32})_5O_8$ solid solution after an incubation period of 200 h implies the occurrence of binodal decomposition.

It has been reported by Yuan and Virkar[3] that there are three stages in the spinodal decomposition of the TiO_2–SnO_2 system. The first stage corresponds to evolution of satellite peaks resulting from concentration fluctuation. In the second stage, the time evolution of Bragg peaks for two separated phases is observed, and formation of interfaces and grain-growth proceed. Interface dislocations should be introduced in the third stage. The first stage of the spinodal decomposition of the $Li(Fe_{0.5}Al_{0.5})_5O_8$ solid solution could not be identified until 10 h annealing at 1000 °C, or 40 h at 950 °C because of significant overlap of the satellite peaks with the main peak. The change in XRD peaks of the $Li(Fe_{0.5}Al_{0.5})_5O_8$ solid solution after 20 h at 1000 °C, and 60 h at 950 °C, as shown in Figs. 3 and 4, corresponds to the second stage of the spinodal decomposition. As the kinetics of the spinodal decomposition is diffusion-controlled, decomposition is promoted at higher temperatures.

Magnetic properties

Fig. 7 shows the magnetic properties of $Li(Fe_xAl_{1-x})_5O_8$ solid solutions before annealing as a function of composition. Magnetization curves for the samples with $x \geqslant 0.4$ revealed hysteresis loops, thus indicating that they were ferrimagnetic. The saturation magnetization, remnant magnetization and coercive force increased with increasing content of magnetic Fe^{3+} ion. An especially notable increase in the saturation magnetization was observed for the samples with $x \geqslant 0.7$.

Fig. 8 shows the variation in the magnetic properties of the $Li(Fe_{0.5}Al_{0.5})_5O_8$ solid solution annealed at 1000 °C inside the chemical spinodal as a function of annealing time. As is evident from the figure, the coercive force increased from 0.8 to 7.2 kA m^{-1} by annealing. An increase up to 8.6 kA m^{-1} was observed by annealing at 950 °C (Fig. 9). The coercive force of the $Li(Fe_{0.5}Al_{0.5})_5O_8$ solid solution increased abruptly in the second stage of the spinodal decomposition, in which the interface of the two separated phases appear. In contrast, as seen in Fig. 10, the coercive force of the $Li(Fe_{0.68}Al_{0.32})_5O_8$ solid solution remained constant at a value of about 2.4 kA m^{-1} during annealing at 1000 °C, outside the chemical spinodal. Figs. 8, 9 and 10 show that the saturation magnetization and remnant magnetization of both $Li(Fe_{0.5}Al_{0.5})_5O_8$ and $Li(Fe_{0.68}Al_{0.32})_5O_8$ solid solutions increased with annealing time. This increase in magnetization is ascribed to the formation of a solid solution with high Fe content by the phase separation, which is expected from Fig. 7 to have a high magnetization value.

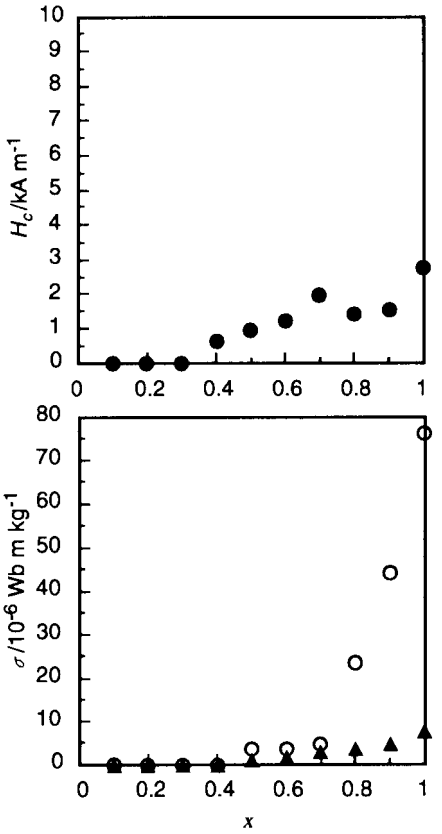

Fig. 7 Magnetic properties of single-phase $Li(Fe_xAl_{1-x})_5O_8$ solid solutions as a function of composition. ● Coercive force (H_c), ○ saturation magnetization (σ_s), ▲ remnant magnetization (σ_r).

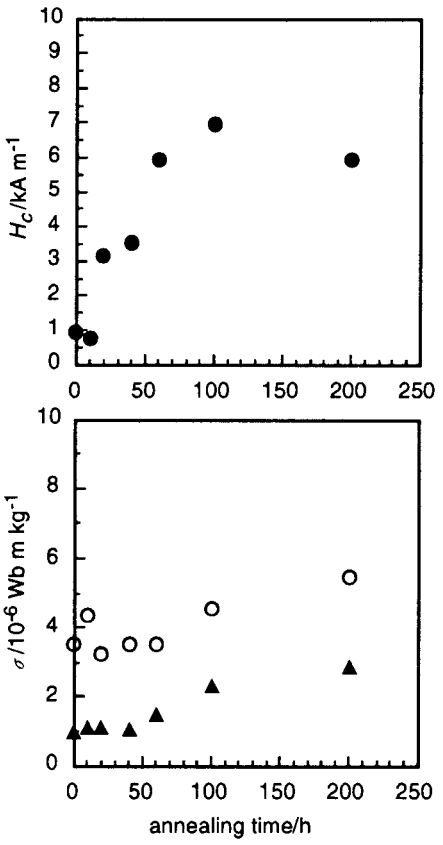

Fig. 8 Variation in magnetic properties of the $Li(Fe_{0.5}Al_{0.5})_5O_8$ solid solution with annealing time at 1000 °C. ● Coercive force (H_c), ○ saturation magnetization (σ_s), ▲ remnant magnetization (σ_r).

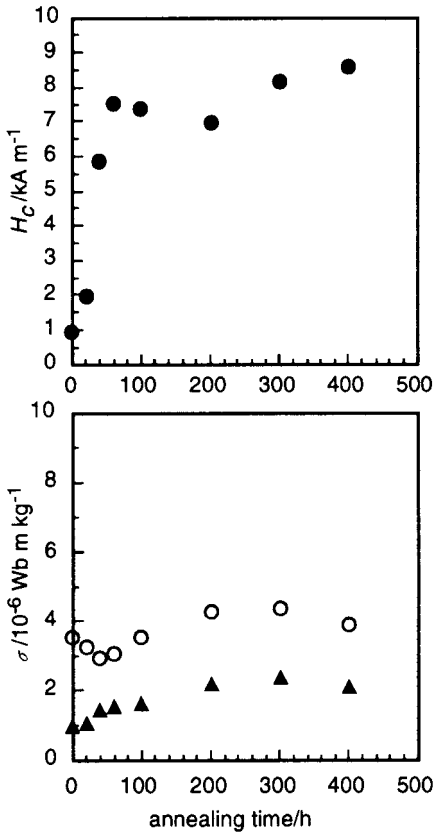

Fig. 9 Variation in magnetic properties of the $Li(Fe_{0.5}Al_{0.5})_5O_8$ solid solution with annealing time at 950 °C. ● Coercive force (H_c), ○ saturation magnetization (σ_s), ▲ remnant magnetization (σ_r).

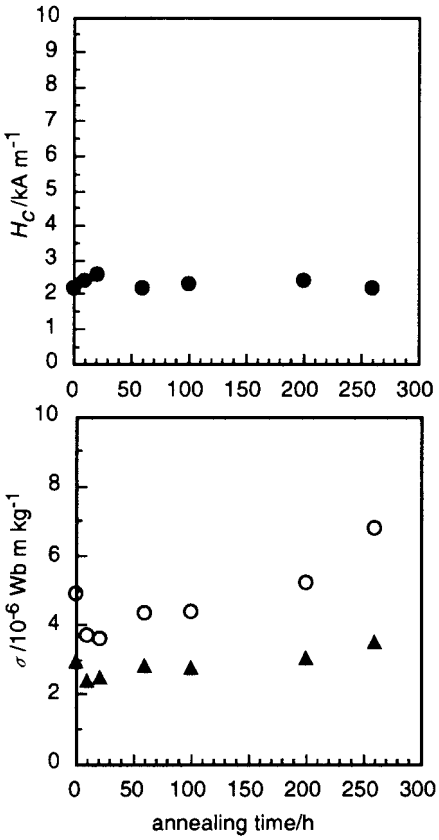

Fig. 10 Variation in magnetic properties of the $Li(Fe_{0.68}Al_{0.32})_5O_8$ solid solution with annealing time at 1000 °C. ● Coercive force (H_c), ○ saturation magnetization (σ_s), ▲ remnant magnetization (σ_r).

The magnetic properties of the polycrystalline ceramics, including the coercive force, are sensitive to crystal defects, width of the domain wall, grain size, grain boundary phases, *etc*. The relative density of the sintered sample was about 85% and did not change after annealing. SEM observation revealed that the average grain size of samples with both $x=0.5$ and 0.68 remained constant at a value of about 5 μm during annealing. The increase in the coercive force for the $Li(Fe_{0.5}Al_{0.5})_5O_8$ solid solution would therefore result from the change in microstructure within the grain, *i.e.* spinodal decomposition. Hirano *et al.*[7] achieved an improvement in the coercive force of sol–gel derived $CoFe_2O_4$–Co_3O_4 films by spinodal decomposition. In the spinodally decomposed films, the lamellar structure consisting of a Co-rich non-magnetic phase and an Fe-rich magnetic phase was observed with a wavelength of 2–5 nm. Spinodally decomposed $Li(Fe_{0.5}Al_{0.5})_5O_8$ is supposed to have a similar modulated microstructure with a non-magnetic Al-rich phase and a magnetic Fe-rich phase. The Al-rich phase may pin the movement of magnetic domain walls, leading to an increase in the coercive force.

Conclusions

The phase separation behaviour and the magnetic properties of the $Li(Fe_xAl_{1-x})_5O_8$ system were examined. The conclusions obtained can be summarized as follows.

(1) The chemical spinodal curve was successfully estimated on the basis of the method of Cook and Hilliard.

(2) The single-phase solid solution $Li(Fe_{0.5}Al_{0.5})_5O_8$ exhibited phase separation with the continuous variation in composition after annealing at 1000 and 950 °C, implying the occurrence of the spinodal decomposition, while the $Li(Fe_{0.68}Al_{0.32})_5O_8$ single-phase solid solution decomposed binodally after annealing at 1000 °C.

(3) The single-phase solid solutions $Li(Fe_xAl_{1-x})_5O_8$ with $x \geqslant 0.4$ were ferrimagnetic.

(4) The coercive force of the $Li(Fe_{0.5}Al_{0.5})_5O_8$ solid solution increased significantly with development of phase separation, probably because of the modulated structure resulting from the spinodal decomposition, while the binodally decomposed $Li(Fe_{0.68}Al_{0.32})_5O_8$ solid solution exhibited no change in the coercive force.

References

1 A. H. Schultz and V. S. Stubican, *Philos. Mag*., 1968, **18**, 929.
2 M. W. Park, T. E. Mitchell and A. H. Heuer, *J. Mater. Sci*., 1976, **11**, 1227.
3 T. C. Yuan and A. V. Virkar, *J. Am. Ceram. Soc*., 1988, **71**, 12.
4 S. Arakawa, K. Mogi, K. Kikuta, T. Yogo, Y. Seki, M. Kawamoto and S. Hirano, *J. Am. Ceram. Soc*., 1997, **80**, 2864.
5 M. Takahashi, J. R. C. Guimaraes and M. E. Fine, *J. Am. Ceram. Soc*., 1971, **54**, 291.
6 M. Takahashi and M. E. Fine, *J. Am. Ceram. Soc*., 1970, **53**, 633.
7 S. Hirano, T. Yogo, K. Kikuta, E. Asai, K. Sugiyama and H. Yamamoto, *J. Am. Ceram. Soc*., 1993, **76**, 1788.
8 J. Chen, Q. Tian and A. V. Virkar, *J. Am. Ceram. Soc*., 1992, **75**, 809.
9 M. Miura, T. Yogo and S. Hirano, *J. Mater. Sci*., 1993, **28**, 3859.
10 M. Miura, T. Yogo and S. Hirano, *J. Ceram. Soc. Jpn*., 1993, **101**, 793.
11 A. H. Schultz and V. S. Stubican, *J. Am. Ceram. Soc*., 1970, **53**, 613.
12 D. W. Strickler and R. Roy, *J. Am. Ceram. Soc*., 1961, **44**, 225.
13 S. J. Kim, Z. C. Chen and A. V. Virkar, *J. Am. Ceram. Soc*., 1988, **71**, C428.
14 G. M. Argentina and P. D. Baba, *IEEE Trans. Microwave Theory Tech*., 1974, **22**, 652.
15 R. K. Mishra and G. Thomas, *J. Am. Ceram. Soc*., 1979, **62**, 293.
16 R. G. West and A. C. Blankenship, *J. Am. Ceram. Soc*., 1967, **50**, 343.
17 F. F. Y. Wang, R. L. Gravel and M. Kestigian, *IEEE Trans. Magn*., 1968, **4**, 55.
18 G. Bandyopadhyay and R. M. Fulrath, *J. Am. Ceram. Soc*., 1974, **57**, 182.
19 H. E. Cook and J. E. Hilliard, *Trans. AIME*, 1965, **233**, 142.

Paper 8/01925H; *Received* 9*th March*, 1998